Inorganic Chemistry
Article

Inorg. Chem. **XXXX**, *XXX*, 000–000 **A**
DOI: 10.1021/ic100641j

Structural, Spectroscopic, and Multiconfigurational Quantum Chemical Investigations of the Electron-Rich Metal−Metal Triple-Bonded $Tc_2X_4(PMe_3)_4$ (X = Cl, Br) Complexes

Frederic Poineau,*,† Paul M. Forster,† Tanya K. Todorova,‡ Laura Gagliardi,‡,§ Alfred P. Sattelberger,*,†,∥ and Kenneth R. Czerwinski†

†*Department of Chemistry, University of Nevada Las Vegas, Las Vegas, Nevada 89154,* ‡*Department of Physical Chemistry, University of Geneva, CH-1211, Geneva, Switzerland,* §*Department of Chemistry and Supercomputing Institute, University of Minnesota, Minneapolis, Minnesota 55455, and* ∥*Energy Engineering and Systems Analysis Directorate, Argonne National Laboratory, Argonne, Illinois 60439*

Received April 4, 2010

The compounds $Tc_2Cl_4(PMe_3)_4$ and $Tc_2Br_4(PMe_3)_4$ were formed from the reaction between $(n\text{-}Bu_4N)_2Tc_2X_8$ (X = Cl, Br) and trimethylphosphine. The Tc(II) dinuclear species were characterized by single-crystal XRD, UV−visible spectroscopy, and cyclic voltammetry techniques, and the results are compared to those obtained from density functional theory and multiconfigurational (CASSCF/CASPT2) quantum chemical studies. The compound $Tc_2Cl_4(PMe_3)_4$ crystallizes in the monoclinic space group *C*2/*c* [*a* = 17.9995(9) Å, *b* = 9.1821(5) Å, *c* = 17.0090(9) Å, β = 115.4530(10)°] and is isostructural to $M_2Cl_4(PMe_3)_4$ (M = Re, Mo, W) and to $Tc_2Br_4(PMe_3)_4$. The metal−metal distance (2.1318(2) Å) is similar to the one found in $Tc_2Br_4(PMe_3)_4$ (2.1316(5) Å). The calculated molecular structures of the ground states are in excellent agreement with the structures determined experimentally. Calculations of effective bond orders for $Tc_2X_8^{2-}$ and $Tc_2X_4(PMe_3)_4$ (X = Cl, Br) indicate stronger π bonds in the Tc_2^{4+} core than in Tc_2^{6+} core. The electronic spectra were recorded in benzene and show a series of low intensity bands in the range 10 000−26 000 cm^{-1}. Assignment of the bands as well as computing their excitation energies and intensities were performed at both TD-DFT and CASSCF/CASPT2 levels of theory. Calculations predict that the lowest energy band corresponds to the $\delta^* \rightarrow \sigma^*$ transition, the difference between calculated and experimental values being 228 cm^{-1} for X = Cl and 866 cm^{-1} for X = Br. The next bands are attributed to $\delta^* \rightarrow \pi^*$, $\delta \rightarrow \sigma^*$, and $\delta \rightarrow \pi^*$ transitions. The cyclic voltammograms exhibit two reversible waves and indicate that $Tc_2Br_4(PMe_3)_4$ exhibits more positive oxidation potentials than $Tc_2Cl_4(PMe_3)_4$. This phenomenon is discussed and ascribed to stronger metal (d) to halide (d) back bonding in the bromo complex. Further analysis indicates that Tc(II) dinuclear species containing π-acidic phosphines are more difficult to oxidize, and a correlation between oxidation potential and phosphine acidity was established.

Introduction

Group VI and VII transition metal dinuclear complexes with multiple metal−metal bonds and mixed halogeno−tertiary phosphine ligands have contributed significantly to our understanding of metal−metal bonding in molecular compounds. In these systems, the M_2^{n+} unit (n = 4, 5, 6) can exhibit bond orders between three and four, and $Re_2Cl_4(PR_3)_4$, $Re_2Cl_5(PR_3)_3$, and $Re_2Cl_6(PR_3)_2$ (R = alkyl) are archetypal compounds of this family.[1] The synthesis of these rhenium dinuclear species involves the reaction between $(n\text{-}Bu_4N)_2Re_2X_8$ (X = Cl, Br) and tertiary phosphines in organic solvents under a variety of conditions. Historically, the first halogenophosphine rhenium(III) quadruply bonded dinuclear complex to be structurally characterized was $Re_2Cl_6(PEt_3)_2$, and the first "electron-rich" triply bonded ones were $Re_2Cl_4(PR_3)_4$ (R_3 = Et_3, n-Pr_3, Et_2Ph, $EtPh_2$, $MePh_2$).[2,3] Currently, more than 50 metal−metal bonded rhenium dinuclear species with phosphine ligands are known and have been structurally characterized.[1] Analyses of the structures and spectroscopic properties of these multiply bonded rhenium dinuclear species have facilitated a better understanding of the nature and influence of the δ bond on the dirhenium unit.

Studies on the technetium analogs are of a more recent vintage; relatively few metal−metal bonded dinuclear species

*To whom correspondence should be addressed. E-mail: asattelberger@anl.gov (A.P.S.) and poineauf@unlv.nevada.edu (F.P.).

(1) Walton, R. A. In *Multiple Bonds between Metal Atoms*, 3rd ed.; Cotton, F. A., Murillo, C. A., Walton, R. A., Eds.; Springer: New York, 2005, Chapter 8.

(2) Cotton, F. A.; Foxman, B. M. *Inorg. Chem.* **1968**, *7*, 2135–2140.

(3) Ebner, J. R.; Walton, R. A. *Inorg. Chem.* **1975**, *14*, 1987–1992.

of this radioelement have been synthesized and characterized. Technetium dinuclear species containing phosphine ligands and having bond orders of 3 and 3.5 represent one of the larger subgroups of Tc metal−metal bonded complexes.[4−6] Complexes with the general formula $Tc_2Cl_4(PR_3)_4$ (R_3 = Et_3, n-Pr_3, Me_2Ph, $MePh_2$) contain the electron-rich $\sigma^2\pi^4\delta^2\delta^{*2}$ triple bond and have been characterized by X-ray diffraction, NMR, electrochemistry, and spectroscopic techniques.[7]

Spectroscopic measurements indicate that the $Tc_2Cl_4(PR_3)_4$ compounds exhibit a low energy band that might logically be attributed to the $\delta^* \rightarrow \sigma^*$ transition, based on assignments proposed for their rhenium analogs.[8] Cyclic voltammograms exhibit two reversible waves which indicate that compounds with Tc_2^{5+} and Tc_2^{6+} cores are accessible. Compounds with a Tc_2^{5+} core (e.g., $Tc_2Cl_5(PMe_2Ph)_3$ and $[Tc_2Cl_4(PMe_2Ph)_4][PF_6]$) were previously synthesized from $Tc_2Cl_4(PMe_2Ph)_4$.[9] Attempts to obtain a quadruply bonded dinuclear complex via two-electron oxidation of $Tc_2Cl_4(PR_3)_4$ (R_3 = Et_3, n-Pr_3, Me_2Ph, $MePh_2$) or reaction of $(n\text{-}Bu_4N)_2Tc_2Cl_8$ with an alkyl phosphine were not successful. In an earlier publication by one of the current authors, it was proposed that $Tc_2Cl_8^{2-}$ undergoes metal−metal scission in the presence of excess phosphine to yield mononuclear Tc species, but this aspect of the chemistry was not pursued.[7]

The electronic structures of multiply metal−metal bonded dinuclear technetium complexes, as well as the influence of ligands on the Tc−Tc core unit, are not well understood. For example, the Tc−Tc separation in the triply bonded dimer, $Tc_2Cl_4(PMe_2Ph)_4$, is shorter than the one in quadruply bonded $(n\text{-}Bu_4N)_2Tc_2Cl_8$, and the Tc−Tc separation in $Tc_2(O_2CCH_3)_4Cl_2$ is larger than in $(n\text{-}Bu_4N)_2Tc_2Cl_8$. These results have been explained qualitatively, but no theoretical studies have addressed them.[10] In recent work on the quadruply bonded dinuclear species, $(n\text{-}Bu_4N)_2Tc_2X_8$ (X = Cl, Br), we determined the structure of the $[Tc_2Br_8]^{2-}$ unit in $(n\text{-}Bu_4N)_2Tc_2Br_8 \cdot 4[(CH_3)_2CO]$ and calculated the energies of the low lying $\delta \rightarrow \delta^*$ transitions using multiconfigurational quantum chemical techniques.[11]

The focus of the present work is on the synthesis and characterization of the triply bonded technetium(II) species containing trimethylphosphine, PMe_3. We have also investigated some aspects of the formation of $Tc_2X_4(PMe_3)_4$ from the reaction between $(n\text{-}Bu_4N)_2Tc_2X_8$ (X = Cl, Br) and trimethylphosphine. These new compounds were characterized by single crystal XRD, UV−visible spectroscopy, and cyclic voltammetry techniques. The results were compared to those obtained from density functional theory (DFT) and multiconfigurational quantum chemical studies using the complete active space SCF (CASSCF) method, followed by second order perturbation theory (CASPT2). The influence of ligands (phosphines and halides) on the Tc−Tc separation in $Tc_2X_4(PMe_3)_4$ (X = Cl, Br) and on the redox properties of these compounds were also investigated. The electronic structures of $Tc_2X_4(PMe_3)_4$ were determined, and the lowest energy electronic transitions in their UV−visible spectra were assigned.

Experimental Section

Caution! *Techetium-99 is a weak β emitter (E_{max} = 292 keV). All manipulations were performed in a laboratory designed for radioactivity using efficient HEPA-filtered fume hoods and Schlenk and glovebox techniques, following locally approved radiochemistry handling and monitoring procedures. Laboratory coats, disposable gloves, and protective eyewear were worn at all times.*

Reagents. Ammonium pertechnetate was purchased from Oak Ridge National Laboratory and purified according to a method previously described.[12] The compounds $(n\text{-}Bu_4N)_2Tc_2X_8$ (X = Cl, Br), $(n\text{-}Bu_4N)TcOCl_4$, *mer*-$TcCl_3(PMe_3)_3$, *trans*-$TcCl_4(PMe_3)_2$, and *trans*-$[TcCl_2(PMe_3)_4]PF_6$ were synthesized according to methods described in the literature.[12−15] All reagent grade solvents (Sigma-Aldrich) were dried over 4 Å molecular sieves, degassed, and stored under an argon atmosphere. Trimethylphosphine (97%, Sigma-Aldrich) was used as received and transferred using anaerobic syringe techniques.

Reaction between $(n\text{-}Bu_4N)_2Tc_2Cl_8$ and PMe_3. A portion of $(n\text{-}Bu_4N)_2Tc_2Cl_8$ (55.1 mg, 0.058 mmol) was placed in a 10 mL Schlenk flask equipped with a gas inlet and connected to a Schlenk line, and 7 mL of CH_2Cl_2 was added via syringe. After dissolution of the solid, PMe_3 (150 μL, 1.411 mmol) was added under an Ar atmosphere via syringe. The green solution turned brown, and a yellow solid **1** immediately precipitated. The suspension was carefully transferred into a 10 mL glass centrifuge tube using a glass pipet. After centrifugation, the supernatant was removed, placed in a 10 mL Schlenk flask, and pumped to dryness, whereupon a brown-green solid was obtained. The solid was extracted three times with 1.5 mL of toluene (3 × 1.5 mL). The toluene extracts were combined in a Schlenk flask and pumped to dryness; an orange oil was obtained. The oil was then extracted with ∼3 mL of hot hexane, placed in a glass vial, and cooled to −25 °C. After three days, orange flakes (**2**) and dark-green crystals (**3**) were observed at the bottom of the vial. The yellow solid **1** was characterized by EXAFS and UV−visible spectroscopy, which revealed the presence of the $TcCl_6^{2-}$ anion. Single crystal X-ray diffraction on **3** showed the compound to be $Tc_2Cl_4(PMe_3)_4$ (*vide infra*). Yield of **3**: 10.0 mg, 26.9%. UV−visible spectral measurements on the orange flakes (**2**), dissolved in methylene chloride, show its spectrum to be identical to that of independently synthesized *mer*-$TcCl_3(PMe_3)_3$.[13] [See the Supporting Information.]

Reaction between $(n\text{-}Bu_4N)_2Tc_2Br_8$ and PMe_3. The reaction was performed in a manner similar to that described above for $(n\text{-}Bu_4N)_2Tc_2Cl_8$. A portion of $(TBA)_2Tc_2Br_8$ (80 mg, 0.060 mmol) was dissolved in 5 mL of CH_2Cl_2, and PMe_3 (300 μL, 2.822 mmol) was added under Ar. An orange precipitate (**4**) formed immediately after the addition of PMe_3. After centrifugation, evaporation of the supernate, and recrystallization from minimal hexane at −25 °C, dark green crystals of **5** were obtained. XRD and UV−visible measurements show the dark

(4) Sattelberger, A. P. In *Multiple Bonds between Metal Atoms*, 3rd ed.; Cotton, F. A., Murillo, C. A., Walton, R. A., Eds.; Springer: New York, 2005, Chapter 7.
(5) Schwochau, K. *Technetium: Chemistry and Radiopharmaceutical Applications*; Wiley-VCH: Weinheim, Germany, 2000.
(6) Cotton, F. A.; Daniels, L. M.; Haefner, S. C.; Sattelberger, A. P. *Inorg. Chim. Acta* **1999**, *288*, 69–73.
(7) Burns, C. J.; Burrell, A. K.; Cotton, F. A.; Haefner, S. C.; Sattelberger, A. P. *Inorg. Chem.* **1994**, *33*, 2257–2264.
(8) Bursten, B. E.; Cotton, F. A.; Fanwick, P. E.; Stanley, G. G.; Walton, R. A. *J. Am. Chem. Soc.* **1983**, *105*, 2606–2611.
(9) Cotton, F. A.; Haefner, S. C.; Sattelberger, A. P. *Inorg. Chem.* **1996**, *35*, 1831–1838.
(10) Poineau, F.; Sattelberger, A. P.; Czerwinski, K. *J. Coord. Chem.* **2008**, *61*, 2356–2370.
(11) Poineau, F; Gagliardi, L; Forster, P. M.; Sattelberger, A. P.; Czerwinski, K. R. *Dalton Trans.* **2009**, *30*, 5954–5959.
(12) Poineau, F.; Sattelberger, A. P.; Conradson, S. D.; Czerwinski, K. R. *Inorg. Chem.* **2008**, *47*, 1991–1999.
(13) Watson, P. L.; Albanese, J. A.; Calabrese, J. C.; Ovenall, D. W.; Smith, R. G. *Inorg. Chem.* **1991**, *30*, 4638–4643.
(14) Rochon, F. D.; Melanson, R. *Acta Crystallogr., Sect. C.* **1993**, *49*, 1259–1262.
(15) Rochon, F. D.; Kong, P. *Inorg. Chem.* **2000**, *39*, 5757–5762.

green **5** to be $Tc_2Br_4(PMe_3)_4$ (*vide infra*). EXAFS and UV−visible measurements (in CH_2Cl_2) on orange **4** revealed the presence of the $TcBr_6^{2-}$ anion.

Characterization Techniques. X-ray diffraction measurements were performed on a Bruker APEX II diffractometer. Crystallographic tables, a .cif file, and structure determination procedures are provided as Supporting Information.

UV−visible spectra were recorded at room temperature in a 1 cm quartz cell on a Cary 6000i double beam spectrometer. Pure solvent was used in the reference beam. Electrochemical measurements were performed on a CH potentiostat. Cyclic voltammetry measurements were performed at room temperature in CH_2Cl_2 using 0.2 M $(n\text{-}Bu_4N)BF_4$ as a supporting electrolyte. A platinum electrode and platinum wire were used as working and counter electrodes, and a silver wire separated with a frit was used as the reference electrode. Ferrocene was used as a standard.

Quantum chemical calculations were performed using DFT and multiconfigurational complete active space SCF (CASSCF) methods,[16] followed by second-order perturbation theory (CASPT2).[17] Full geometry optimization of the $Tc_2X_4(PMe_3)_4$ (X = Cl, Br) compounds was performed at the DFT level, employing two different exchange correlation functionals, i.e., PBE and PBE0, along with triple-ζ (def2-TZVP) as well as quadruple-ζ (def2-QZVP) valence plus polarization basis sets on all atoms. A quasi-relativistic pseudopotential was used for the Tc atom with 28 core electrons. Time-dependent TDDFT calculations were performed at the optimized geometries in order to assess the vertical electronic excitations. The TURBOMOLE 6.0 program package was used.[18] The CASSCF/CASPT2 calculations were performed with the MOLCAS 7.4 package[19] at the DFT/PBE0/TZVP optimized geometries. The calculations employed two sets of the relativistic all electron ANO-RCC basis sets,[20] one with basis sets of triple-ζ quality (VTZP) and one with quadruple-ζ (VQZP) quality for Tc, Cl, Br, and P. The VTZP basis corresponds to the following contractions: 7s6p4d2f1g for Tc, 5s4p2d1f for Cl and P, and 6s5p3d1f for Br. The VQZP basis corresponds to the contractions: 8s7p5d3f2g1f for Tc, 6s5p3d2f1g for Cl and P, and 7s6p4d2f1g for Br. Double-ζ basis set quality (VDZP) was used for C and H, contracted to 3s2p1d and 2s1p, respectively. Scalar relativistic effects were included using the Douglas−Kroll−Hess Hamiltonian.[21] In the CASSCF calculations, the complete active space contains 14 electrons in 12 active orbitals (14/12). This space comprises one 4dσ, two 4dπ, and one 4dδ Tc−Tc bonding orbital and the corresponding antibonding orbitals and two Tc−L (L = Cl, Br, and P) σ bonding and corresponding antibonding orbitals. In the subsequent CASPT2 calculations, orbitals up to and including the 3d for Tc, 2p for Cl and P, 3p for Br, and 1s for C were kept frozen. With the same approach, we have successfully studied several metal−metal bonded compounds in the past.[11,22−25] The computational costs arising from the two-electron integrals were drastically reduced by employing the Cholesky decomposition (CD) technique in all CASSCF/CASPT2 calculations[26−28] combined with the local exchange (LK) screening.[29]

X-ray absorption fine structure spectroscopy (XAFS) measurements were performed at the Advanced Photon Source at Argonne National Laboratory. Compounds were diluted in boron nitride (1%). Spectra were recorded at the Tc−K edge (21044 eV) in the fluorescence mode using a 13 element detector. Fitting procedures are described in the Supporting Information.

^{99}Tc concentrations were determined by liquid scintillation counting using a Packard 2500 scintillation analyzer. The scintillation cocktail was ULTIMA GOLD AB (Packard).

Results and Discussion

Synthesis of $Tc_2X_4(PMe_3)_4$ from $(n\text{-}Bu_4N)_2Tc_2X_8$. In a previous publication, the authors successfully synthesized compounds with formula $Tc_2Cl_4(PR_3)_4$ (R_3 = Et_3, $n\text{-}Pr_3$, Me_2Ph, $MePh_2$) by sonication of *trans*-$TcCl_4(PR_3)_2$ with zinc metal in THF or benzene.[7] In the present work, attempts to synthesize $Tc_2Cl_4(PMe_3)_4$ via sonication of the known *trans*-$TcCl_4(PMe_3)_2$[14] in benzene with zinc were unsuccessful. The analogous rhenium complexes $Re_2X_4(PR_3)_4$ (X = Cl, Br, I; R_3 = Me_3, Et_3, $n\text{-}Pr_3$, Et_2Ph, $MePh_2$) are obtained in high yield from the reaction between $Re_2X_8^{2-}$ and the corresponding phosphines.[3,30−32] Encouraged by these results, the reaction between $Tc_2X_8^{2-}$ and trimethylphosphine was investigated.

Several outcomes are possible when tertiary phosphines are reacted with multiply metal−metal bonded dinuclear species: substitution, reduction, disproportionation, or scission of the metal−metal bond. For rhenium, the mechanism depends on the solvent, e.g., when $Re_2Cl_8^{2-}$ is reacted with a tertiary phosphine in benzene, disproportionation occurs ($3Re_2^{6+} \rightarrow 2Re_2^{5+} + 2Re^{4+}$), while in alcohol, reduction of Re_2^{6+} to Re_2^{4+} is observed.[3,30,33] When $Os_2Cl_8^{2-}$ salts are reacted with PMe_3, scission of the Os_2^{6+} unit occurs and monomeric Os^{2+} and Os^{3+} species are formed.[34] As one molybdenum example, $Mo_2Cl_4(PMe_3)_4$ is formed through the substitution of $Mo_2Cl_8^{4-}$ with PMe_3.[35]

In the present work, the formation of Tc^{4+} and Tc_2^{4+} species, i.e., TcX_6^{2-} and $Tc_2X_4(PMe_3)_4$, from $Tc_2X_8^{2-}$ (X = Cl, Br) indicates that disproportionation of the Tc_2^{6+} unit is occurring. In order to investigate this process further, a UV−visible study was performed shortly after the addition of PMe_3 to a $Tc_2Cl_8^{2-}$ solution. Trimethylphosphine (15 μL, 0.1411 mmol) was added to 1 mL of a 0.0045 M $Tc_2Cl_8^{2-}$ dichloromethane solution in a centrifuge tube. Precipitation of a yellow solid occurred. The

(16) Roos, B. O.; Taylor, P. R.; Siegbahn, P. E. M. *Chem. Phys.* **1980**, *48*, 157–173.
(17) Andersson, K.; Malmqvist, P. A.; Roos, B. O. *J. Chem. Phys.* **1992**, *96*, 1218–1226.
(18) Ahlrichs, R.; Baer, M.; Haeser, M.; Horn, H.; Koelmel, C. *Chem. Phys. Lett.* **1989**, *162*, 165–169.
(19) Karlström, G.; Lindh, R.; Malmqvist, P.-Å.; Roos, B. O.; Ryde, U.; Veryazov, V.; Widmark, P.-O.; Cossi, M.; Schimmelpfennig, B.; Neogrady, P.; Seijo, L. *Comput. Mater. Sci.* **2003**, *287*, 222–239.
(20) Roos, B. O.; Lindh, R.; Malmqvist, P.-A.; Veryazov, V.; Widmark, P.-O. *J. Phys. Chem. A* **2005**, *109*, 6575–6579.
(21) Hess, B. A. *Phys. Rev. A* **1986**, *33*, 3742–3748.
(22) Ferrante, F.; Gagliardi, L.; Bursten, B. E.; Sattelberger, A. P. *Inorg. Chem.* **2005**, *44*, 8476–8480.
(23) Gagliardi, L.; Roos, B. O. *Inorg. Chem.* **2003**, *42*, 1599–1603.
(24) Roos, B. O.; Borin, A.; Gagliardi, L. *Angew. Chem., Int. Ed.* **2007**, *46*, 1469–1472.
(25) Brynda, M.; Gagliardi, L.; Roos, B. O. *Chem. Phys. Lett.* **2009**, *471*, 1–10.
(26) Aquilante, F.; Malmqvist, P. A.; Pedersen, T. B.; Ghosh, A.; Roos, B. O. *J. Chem. Theory Comput.* **2008**, *4*, 694–702.
(27) Aquilante, F.; Pedersen, T. B.; Lindh, R.; Roos, B. O.; De Meras, A. S.; Koch, H. *J. Chem. Phys.* **2008**, *129*, 024113.
(28) Aquilante, F.; Pedersen, T. B.; Gagliardi, L.; Lindh, R. *J. Chem. Phys.* **2009**, *130*, 154107.
(29) Aquilante, F.; Pedersen, T. B.; Lindh, R. *J. Chem. Phys.* **2007**, *126*, 194106.
(30) Root, D. R.; Blevins, C. H.; Lichtenberger, D. L.; Sattelberger, A. P.; Walton, R. A. *J. Am. Chem. Soc.* **1986**, *108*, 953–959.
(31) Brant, P.; Walton, R. A. *Inorg. Chem.* **1978**, *17*, 2674–2677.
(32) Angaridis, P.; Cotton, F. A.; Dikarev, E. V.; Petrukhina, M. A. *Polyhedron* **2001**, *20*, 755–765.
(33) Cotton, F. A.; Dikarev, E. V.; Petrukhina, M. A. *Inorg. Chem.* **1999**, *38*, 3384–3389.
(34) Fanwick, P. E.; Fraser, I. F.; Tetrick, S. M.; Walton, R. A. *Inorg. Chem.* **1987**, *26*, 3786–3791.
(35) Cotton, F. A.; Extine, M. W.; Felthouse, T. R.; Kolthammer, B. W.; Lay, D. G. *J. Am. Chem. Soc.* **1981**, *103*, 4040–4045.

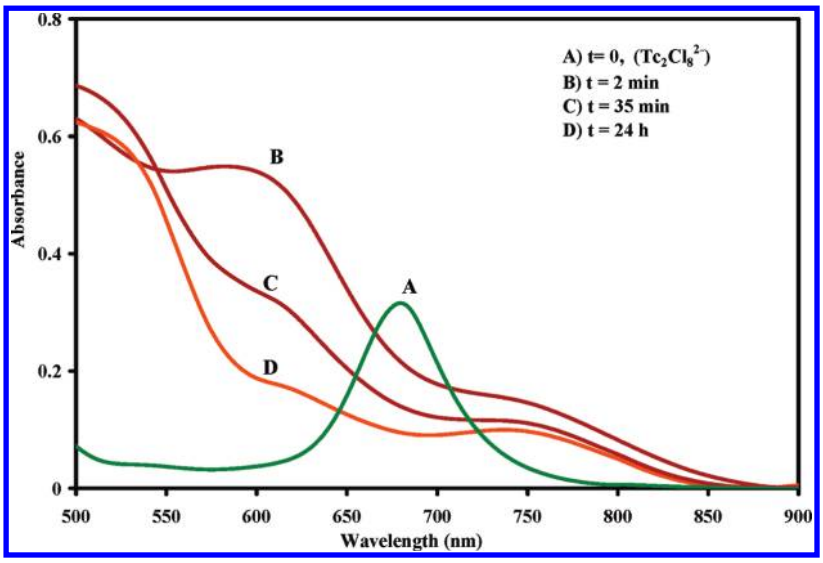

Figure 1. UV−visible spectra of a 0.0045 M (n-$Bu_4N)_2Tc_2Cl_8$ solution in CH_2Cl_2 before and after the addition of PMe_3. A spectrum before PMe_3 addition (green curve) was recorded after dilution (1/20), while spectra after PMe_3 addition were recorded without dilution as a function of time.

solution was centrifuged (20 s), and the supernate was immediately transferred into a 1 cm quartz cuvette for UV−visible measurements. The yellow precipitate was dissolved in acetonitrile, and a UV−visible measurement confirmed that it was, in fact, $TcCl_6^{2-}$. Spectral scans of the solution were recorded before and after the addition of PMe_3 (Figure 1). Two minutes after the addition of PMe_3, examination of the spectrum in the region 500−900 nm revealed the complete disappearance of the band at 678 nm ($\delta \rightarrow \delta^*$ transition of $Tc_2Cl_8^{2-}$) and the appearance of bands centered at 750 and 590 nm. Further measurements show that the band at 590 nm rapidly decreases in intensity while the band at 750 nm persists 24 h after the addition.

Identification of the Tc species was performed using the position and intensity of the bands characteristic of the known mononuclear and dinuclear Tc chloro-trimethylphosphine complexes (i.e., *mer*-$TcCl_3(PMe_3)_3$,[13] *trans*-$TcCl_4(PMe_3)_2$,[14] *trans*-$[TcCl_2(PMe_3)_4][PF_6]$,[15] *trans*-$TcCl_2(PMe_3)_4$,[36] and $Tc_2Cl_4(PMe_3)_4$). The spectroscopic data are presented in Table 1 and in the Supporting Information. The low intensity band at 750 nm is attributed to $Tc_2Cl_4(PMe_3)_4$ (see the Spectroscopy section). The concentration of $Tc_2Cl_4(PMe_3)_4$ calculated after 24 h indicates that this compound represents ~30% of the total Tc concentration. The more intense band at 590 nm was attributed to *trans*-$TcCl_4(PMe_3)_2$. The stability of $TcCl_4(PMe_3)_2$ and $Tc_2Cl_4(PMe_3)_4$ was studied in CH_2Cl_2 in the presence of PMe_3. The results indicate that *trans*-$TcCl_4(PMe_3)_2$ is rapidly converted to *mer*-$TcCl_3(PMe_3)_3$, while $Tc_2Cl_4(PMe_3)_4$ is stable for 24 h. The decrease of the band at 590 nm is likely due to conversion of *trans*-$TcCl_4(PMe_3)_2$ to *mer*-$TcCl_3(PMe_3)_3$ and explains the presence of the latter compound as a product in the synthesis of $Tc_2Cl_4(PMe_3)_4$.

To summarize, the present study shows that dinuclear Tc_2^{4+} and mononuclear Tc^{4+} species are observed immediately after reaction of $Tc_2Cl_8^{2-}$ with PMe_3 in dichloromethane and indicate that a disproportionation ($2Tc_2^{6+} \rightarrow Tc_2^{4+} + 2Tc^{4+}$) is the genesis of $Tc_2Cl_4(PMe_3)_4$ formation.

(36) Poineau, F.; Sattelberger, A. P.; Czerwinski, K. R. To be published.

Table 1. Absorption Maxima (nm) and Absorption Coefficients (ε, M^{-1} cm^{-1}) Determined for Various Tc Chloro-Phosphine Complexes in Dichloromethane

species	wavelength nm, (ε, M^{-1} cm^{-1})
trans-$TcCl_4(PMe_3)_2$	593 (2554), 330 (6965)
mer-$TcCl_3(PMe_3)_3$	462 (1701), 365 (3210),
trans-$TcCl_2(PMe_3)_4[PF_6]$	436 (2726), 395 (1857), 317 (2695)
trans-$TcCl_2(PMe_3)_4$	390 (1603), 447 (457)
$Tc_2Cl_4(PMe_3)_4$	740 (22), 614 (24), 448 (63)

What remains unclear is how $TcCl_6^{2-}$ (or $TcBr_6^{2-}$) is formed at the earliest stage of the reaction.

Molecular Structure. The compound $Tc_2Cl_4(PMe_3)_4$ (**3**) crystallizes in the monoclinic space group $C2/c$ and is isostructural to $M_2Cl_4(PMe_3)_4$ (M = Re, Mo, W)[35,37] and to $Tc_2Br_4(PMe_3)_4$.[38] It exhibits the eclipsed conformation with D_{2d} symmetry, the individual *trans*-$TcCl_2(PMe_3)_2$ units being nonplanar due to intramolecular repulsion (Figure 2). The complex exhibits a small amount (< 1%) of positional disordering in its crystallographic structure; i.e., the Tc_2^{4+} units can point in either of two perpendicular orientations (see the Supporting Information). In the major orientation, Tc1−Tc2 coincides with a crystallographic C2 axis. It is the first time that this type of disorder has been observed in an $M_2Cl_4(PMe_3)_4$ (M = Re, Mo, W) compound.

The metal−metal distance (2.1318(2) Å, Figure 2) in $Tc_2Cl_4(PMe_3)_4$ is consistent with presence of an electron-rich $\sigma^2\pi^4\delta^2\delta^{*2}$ triple bond and is essentially identical to the one found in $Tc_2Br_4(PMe_3)_4$ (2.1316(5) Å).[38] The interatomic distances in $Tc_2Cl_4(PR_3)_4$ (R_3 = Et_3, Me_3, Me_2Ph, $MePh_2$) are presented in Table 2. In these compounds, the Tc−Tc separation varies over a narrow range of 2.127(1) Å (R_3 = Me_2Ph) to 2.138(4) Å (R_3 = $MePh_2$).[7] The relative insensitivity of the Tc_2^{4+} unit to the nature of the coordinating phosphine ligand contrasts with Tc_2^{6+}. For the quadruply bonded dinuclear complexes, an elongation of the Tc−Tc distance is observed on replacing Cl

(37) Cotton, F. A.; Price, A. C.; Vidyasagar, K. *Inorg. Chem.* **1990**, *29*, 5143–5147.

(38) Poineau, F.; Weck, P. F.; Forster, P. M.; Sattelberger, A. P.; Czerwinski, K. R. *Dalton Trans.* **2009**, *46*, 10338–10342.

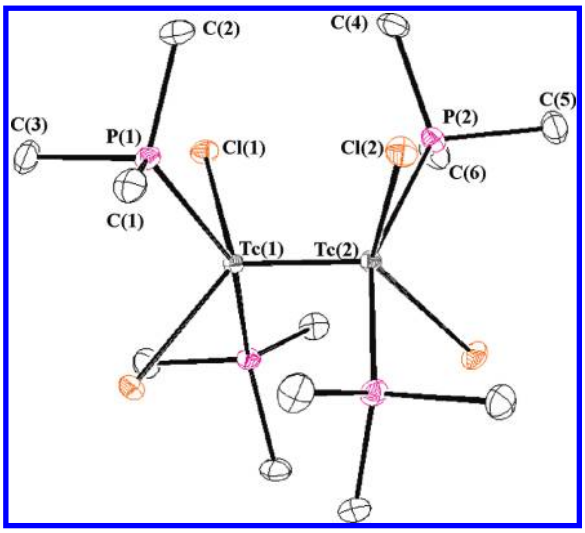

Figure 2. ORTEP representation and selected bond lengths [Å] and angles [deg] for the major orientation (> 99%) of $Tc_2Cl_4(PMe_3)_4$. Hydrogen atoms are omitted for clarity. Tc(1)−Tc(2) = 2.1318(2), Tc(1)−Cl(1) = 2.3852(3), Tc(1)−P(1) = 2.4343(3), Tc(2)−Cl(2) = 2.3865(3), Tc(2)−P(2) = 2.4370(3). Tc(2)−Tc(1)−Cl(1) = 113.181(9), Tc(2)−Tc(1)−P(1) = 102.148(8), Cl(1)−Tc(1)−P(1) = 85.285(11), Tc(1)−Tc(2)−Cl(2) = 113.375(8), Tc(1)−Tc(2)−P(2) = 101.925(8), Cl(2)−Tc(2)−P(2) = 85.330(12).

Table 2. Average Interatomic Distances (Å) in $Tc_2Cl_4(PR_3)_4$ (R_3 = Me_3, Et_3, Me_2Ph, $MePh_2$)

$Tc_2Cl_4(PR_3)_4$	Tc−Tc (Å)	Tc−Cl (Å)	Tc−P (Å)
$R_3 = Me_3$	2.1318(2)	2.3858(4)	2.4356(4)
$R_3 = Et_3$	2.133(3)	2.488(4)	2.448(3)
$R_3 = Me_2Ph$	2.127(1)	2.394(2)	2.446(2)
$R_3 = MePh_2$	2.1384(5)	2.365(2)	2.480(2)

with Br (2.147(4)−2.1625(9) Å) or with a carboxylate ligand (2.147(4)−2.19(2) Å).[10,11] Currently, no quadruply bonded technetium(III) dinuclear species containing tertiary phosphine ligands are known.

Further analysis indicates that the Tc−P distances vary between 2.4356(4) Å and 2.480(2) Å, which is consistent with the ones found in monomeric *trans*-dihalo Tc(II) phosphine complexes.[37,39] The Tc−Cl distances vary from 2.365(2) Å ($R_3 = MePh_2$) to 2.488(4) ($R_3 = Et_3$). Except for $Tc_2Cl_4(PEt_3)_4$, the Tc−Cl distances in the Tc(II) dinuclear species are shorter than in the Tc(II) mononuclear complexes. This phenomenon has already been discussed and ascribed to steric congestion in the mononuclear species.[38]

Geometry optimizations of $Tc_2Cl_4(PMe_3)_4$ and $Tc_2Br_4(PMe_3)_4$ performed at the DFT level of theory reveal that the calculated Tc−Tc, Tc−X (X = Cl, Br), and Tc−P bond distances are in excellent agreement with the experimental values. The structural parameters obtained at the DFT/PBE and DFT/PBE0 levels with TZVP and QZVP basis sets are presented in Tables S8 and S11 in the Supporting Information. Calculations confirm the experimental observation that the Tc−Tc bond distance is identical in both complexes (2.12 Å at pbe0/TZVP and 2.11 Å at pbe0/QZVP level). The Tc−Cl distance is 2.38 Å, whereas Tc−Br is significantly longer (2.53 Å). The Tc−P distance

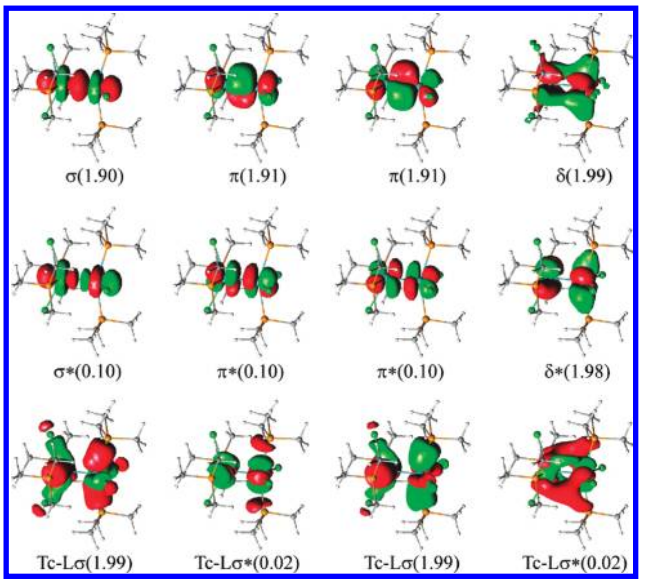

Figure 3. Active orbitals for $Tc_2X_4(PMe_3)_4$ (X = Cl, Br) and their occupation numbers in the ground state.

Table 3. Effective Bond Order, Total Bond Order, and Tc−Tc Distance Calculated (at the VTZP Basis Set Level) for $Tc_2X_8^{2-}$ and $Tc_2X_4(PMe_3)_4$ (X = Cl, Br)[41]

		effective bond order			
compounds	Tc−Tc (Å)	σ	π	δ	total bond order
$Tc_2Cl_8^{2-}$	2.170	0.88	1.68	0.47	3.03
$Tc_2Cl_4(PMe_3)_4$	2.118	0.90	1.81	0.01	2.72
$Tc_2Br_8^{2-}$	2.173	0.88	1.69	0.50	3.07
$Tc_2Br_4(PMe_3)_4$	2.117	0.90	1.81	0.01	2.72

varies in a very narrow range of 2.42−2.44 Å, independent of the basis set or the nature of X.

Electronic Structure. An interesting question in the coordination chemistry of metal−metal bonded complexes is how changes in charge and electronic configuration of the metal in the M_2^{n+} unit affect the metal−metal separation. For the technetium dinuclear species, it might be anticipated that a decrease of bond order moving from a Tc_2^{6+} core to Tc_2^{4+} would be accompanied by an increase in the metal−metal separation; in fact, the opposite is observed, viz., a contraction of the Tc−Tc separation occurs with decreasing bond order. This phenomenon has been qualitatively explained by suggesting that contraction of 4d orbitals with increasing charge on the metal leads to less favorable overlap and somewhat weaker bonds.[11,40] We have performed CASSCF/CASPT2 calculations in order to investigate the electronic structures of the two technetium(II) phosphine compounds and to determine the bond order of the metal−metal bond in each dimer. The CASSCF wave function is analyzed in terms of its natural orbitals and their occupation numbers. The 12 molecular orbitals forming the active space for $Tc_2X_4(PMe_3)_4$ (X = Cl, Br) along with their occupation numbers are presented in Figure 3. The dominant electronic configuration in the $^1A_{1g}$ ground states of $Tc_2Cl_4(PMe_3)_4$ and $Tc_2Br_4(PMe_3)_4$ has a weight of 85%. The two bonding Tc−L orbitals are mainly located on L (L = Cl, Br, and P),

(39) Libson, K.; Doyle, M. N.; Thomas, R. W.; Nelesnik, T.; Woods, M.; Sullivan, J. C.; Elder., R. C.; Deutsch, E. *Inorg. Chem.* **1988**, *27*, 3614–3619.

(40) Cotton, F. A; Dunbar, K. R.; Falvello, L. R.; Tomas, M.; Walton, R. A. *J. Am. Chem. Soc.* **1983**, *105*, 4950–4954.

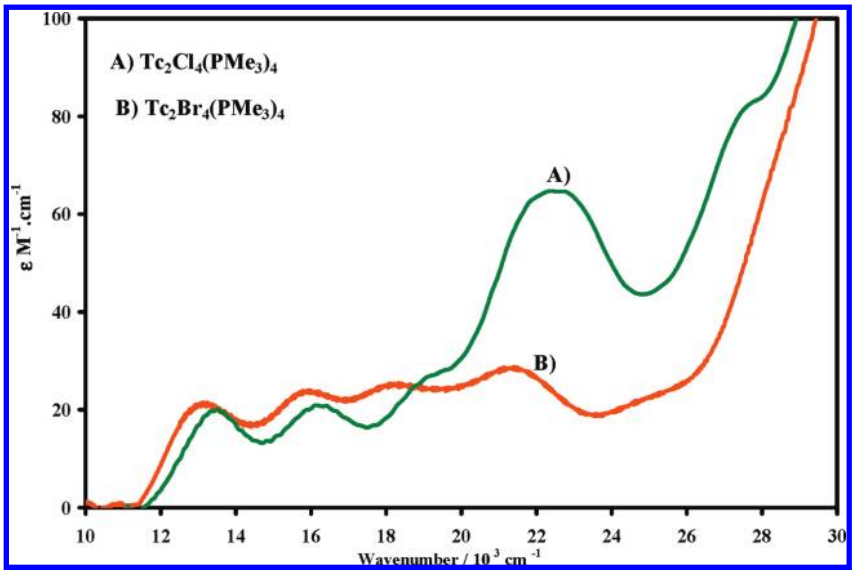

Figure 4. Absorption spectra of $Tc_2X_4(PMe_3)_4$ (X = Cl, Br) in benzene.

Table 4. Experimental Band Maxima (cm^{-1}), Absorption Coefficients ε (M^{-1} cm^{-1}), Assignment, CASPT2 Excitation Energies (cm^{-1}), and Intensities Using the VQZP Basis Set for $Tc_2Cl_4(PMe_3)_4$[a]

experimental	ε, M^{-1} cm^{-1}	assignment	excitation energies	intensity
13 477	19	$\delta^* \rightarrow \sigma^*$	13 249	0
16 129	19	$\delta^* \rightarrow \pi^*$	16 370	0.14×10^{-4}
19 200 (sh)	24	$\delta \rightarrow \sigma^*$	20 744	$< 1.0 \times 10^{-8}$
22 371	54	$\delta \rightarrow \pi^*$	24 163	0.21×10^{-3}
27 777(sh)	68	$\delta \rightarrow \sigma^*$(Tc-L)	27 215	$< 1.0 \times 10^{-8}$

[a] Values calculated using the VTZP basis set, as well as those obtained at TDDFT level, are presented in the Supporting Information.

Table 5. Experimental Band Maxima (cm^{-1}), Absorption Coefficients ε (M^{-1} cm^{-1}), Assignment, CASPT2 Excitation Energies (cm^{-1}), and Intensities Using the VQZP Basis Set for $Tc_2Br_4(PMe_3)_4$[a]

experimental	ε, M^{-1} cm^{-1}	assignment	excitation energies	intensity
13 072	21	$\delta^* \rightarrow \sigma^*$	12 206	0
15 949	24	$\delta^* \rightarrow \pi^*$	16 516	0.17×10^{-4}
18 281	25	$\delta \rightarrow \sigma^*$	19 836	$< 1.0 \times 10^{-8}$
21 436	28	$\delta \rightarrow \pi^*$	24 410	0.14×10^{-3}

[a] Values calculated using the VTZP basis set, as well as those obtained at TDDFT level, are presented in the Supporting Information.

while the corresponding antibonding orbitals have a large contribution from the Tc $4d_{x^2-y^2}$ orbital. The Tc−Tc bonding is quantified in terms of effective bond order (EBO), defined as $(\eta_b - \eta_a)/(\eta_b + \eta_a)$, where η_b is the occupation number for the bonding natural orbital and η_a is the occupation number for the antibonding natural orbital. The occupancy of δ and δ^* orbitals is nearly identical, which gives no contribution to the δ bond (effective bond order of 0.01). The similar occupancy of the σ and two π orbitals indicates that these orbitals have approximately the same strength. The EBO value for the σ bond is 0.90, and the corresponding value for the π bond is 1.81. This results in a total bond order of 2.72. Furthermore, the halide ligand has no effect on metal−metal bonding in the Tc_2^{4+} core; i.e., the effective bond orders in the $Tc_2X_4(PMe_3)_4$ (X = Cl, Br) complexes are identical.

Closer inspection of the Tc−Tc distances in the optimized structures of $Tc_2X_8^{2-}$ and $Tc_2X_4(PMe_3)_4$ (X = Cl, Br) reveals the decrease of the metal−metal distance with the total bond order when moving from Tc_2^{6+} to Tc_2^{4+} and confirms the trend observed experimentally. Effective bond order calculations of the σ, π, and δ components in $Tc_2X_8^{2-}$ and $Tc_2X_4(PMe_3)_4$ (Table 3) indicate that the Tc_2^{4+} core has stronger π bonds than the Tc_2^{6+} core and is consistent with the decrease of the Tc−Tc distance associated with reduction of total bond order in the Tc_2^{4+} unit, assuming the δ bond(s) contributes minimally to the overall bond length in the Tc_2^{6+} and Tc_2^{4+} cores. Thus, once again, simple bond order considerations cannot be used to predict bond lengths, but each component needs to be considered individually.

Spectroscopy. In order to gain additional insight into the electronic structure of $Tc_2X_4(PMe_3)_4$ (X = Cl, Br) complexes, spectroscopic measurements and CASSCF/CASPT2 as well as TD-DFT calculations were performed. Crystals of $Tc_2X_4(PMe_3)_4$ were dissolved in benzene and the UV−visible spectrum recorded between 30 000 cm^{-1} and 10 000 cm^{-1}. The UV−visible spectra (Figure 4) of $Tc_2X_4(PMe_3)_4$ (X = Cl, Br) show a series of five low intensity bands; the bands in the spectrum of the chloro complex being shifted to slightly higher energy relative to those of its bromo analog. In previous studies on the $Tc_2Cl_4(PR_3)_4$ compounds, the lowest energy band was the only one to be assigned and was attributed to the $\delta^* \rightarrow \sigma^*$ transition.[7] Attempts to correlate the position of this transition to the π-acidity of phosphine did not give satisfactory results. In the present work, attribution of unassigned bands in $Tc_2X_4(PMe_3)_4$ (X = Cl, Br) spectra was performed at both the TD-DFT and CASSCF/CASPT2 levels. The experimental and theoretical results are presented in Tables 4 and 5.

Our calculations on $Tc_2X_4(PMe_3)_4$ (X = Cl, Br) also predict that the lowest energy band corresponds to the

(41) Todorova, T. K. Private communication on $Tc_2X_8^{2-}$ (X = Cl, Br) calculations. A numerical optimization of the Tc−Tc bond distances was performed for the ground states of $Tc_2X_8^{2-}$ at the CASPT2 level using the VTZP basis set.

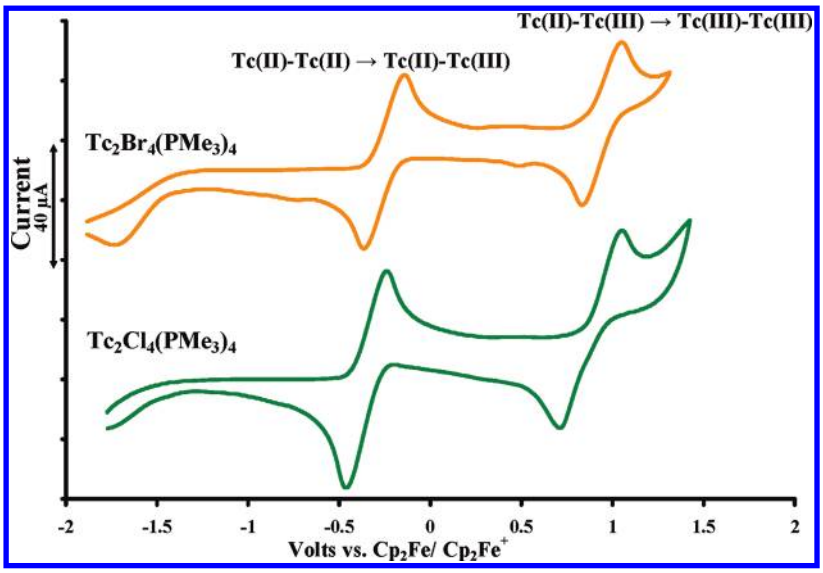

Figure 5. Cyclic voltammograms of $Tc_2X_4(PMe_3)_4$ (X = Cl, Br) in CH_2Cl_2/0.2 M (n-Bu_4N)BF_4 at a scan rate of 200 mV s^0.

Table 6. Formal and Oxidation Potentials (Volts vs Cp_2Fe/Cp_2Fe^+) for the $Tc_2X_4(PMe_3)_4$ (X = Cl, Br) Complexes[a]

$Tc_2X_4(PMe_3)_4$	E^I	E^{II}	$(E^I{}_{1/2})$ox	$(E^{II}{}_{1/2})$ox
X = Cl	−0.335	0.894	−0.344	0.938
X = Br	−0.201	0.984	−0.248	0.957

[a] Values recorded in CH_2Cl_2 using 0.2 M (n-Bu_4N)BF_4 as a supporting electrolyte at a scan rate of 200 mV s^{-1}.

dipole forbidden $\delta^* \rightarrow \sigma^*$ transition; the difference between calculated (at the CASPT2 level with VQZP basis set) and experimental values being 228 cm^{-1} for X = Cl and 866 cm^{-1} for X = Br. The calculations are also able to mimic the red shift of the $\delta^* \rightarrow \sigma^*$ transition observed for the bromo compound, the calculated shift (1043 cm^{-1}) being reasonably close to the experimental one (~400 cm^{-1}). The next band is attributed to the dipole allowed $\delta^* \rightarrow \pi^*$ transition, and its calculated position matches well with the experimental values. Even though this transition is formally allowed, it is very weak (ε = 19 M^{-1} cm^{-1}) as might be anticipated for an excitation between δ- and π-type orbitals.[8] The next transition appears as a shoulder in the $Tc_2Cl_4(PMe_3)_4$ spectrum (~19 200 cm^{-1}) and as a distinct band (18 281 cm^{-1}) in the $Tc_2Br_4(PMe_3)_4$ spectrum; these bands are assigned to the $\delta \rightarrow \sigma^*$ transition. The position of the $\delta \rightarrow \sigma^*$ and $\delta^* \rightarrow \sigma^*$ transitions permits one to estimate the separation between the δ and δ^* orbitals; for the bromo compound, a separation of 0.65 eV is found. For the chloro compound, due to uncertainty of the exact position of the shoulder, an approximate value of 0.71 eV is found.

The higher intensity bands located around 22 000 cm^{-1} are attributed to the $\delta \rightarrow \pi^*$ transition which is allowed in D_{2d} symmetry. The higher intensity of the $\delta \rightarrow \pi^*$ transition is also confirmed theoretically. The positions of the $\delta \rightarrow \pi^*$ and $\delta^* \rightarrow \pi^*$ transitions also provide an opportunity to estimate the separation between the δ and δ^* orbitals. For the bromo compound, the difference is 0.68 eV and in good agreement with one estimated above (i.e., 0.65 eV). For the chlorine compound, the separation is 0.77 or 0.06 eV higher than the one estimated above. The calculated energy gap between those orbitals is 1.15 eV for $Tc_2Cl_4(PMe_3)_4$ and 1.08 eV for $Tc_2Br_4(PMe_3)_4$.

The agreement between experimental and calculated values of the low energy electronic transitions of $Tc_2X_4(PMe_3)_4$ (X = Cl, Br) is impressive and indicates the utility of multiconfiguration quantum chemical methods for analyzing electronic transitions in early metal dinuclear species.

Electrochemistry. Previous electrochemical measurements on metal−metal bonded dinuclear species have shown that the nature of coordinating halides and/or phosphines can affect the redox properties of these compounds.[41−43] Very few electrochemical studies have been performed on technetium complexes. In this context, the $Tc_2X_4(PMe_3)_4$ (X = Cl, Br) complexes were analyzed by cyclic voltammetry and their redox properties compared to the $Tc_2Cl_4(PR_3)_4$ (R_3 = Et_3, n-Pr_3, Me_2Ph, $MePh_2$) analogs.

The two compounds were dissolved in CH_2Cl_2 and their respective cyclic voltammograms recorded on a platinum electrode at various scan rates [100 mV s^{-1} to 300 mV s^{-1}]. As was the case with their rhenium homologs, the cyclic voltammograms (Figure 5) exhibit two reversible waves.[40] In the oxidation of the Tc_2^{4+} unit, one electron is successively removed from the δ^* orbital; the more cathodic oxidation wave (I) is associated with the $Tc_2^{4+} \rightarrow Tc_2^{5+} + e^-$ reaction, while the more anodic wave (II) corresponds to the $Tc_2^{5+} \rightarrow Tc_2^{6+} + e^-$ reaction. The oxidation potentials for these reactions, respectively $(E^I{}_{1/2})$ox and $(E^{II}{}_{1/2})$ox, are measured at half of the peak current. The formal potentials for the Tc_2^{5+}/Tc_2^{4+} and Tc_2^{6+}/Tc_2^{5+} couples (respectively E^I and E^{II}) are defined as $E = [Ep_a + Ep_c]/2$; Ep_a and Ep_c are the potentials at the maximum current for anodic and cathodic waves. An analysis of Table 6 indicates that $Tc_2Br_4(PMe_3)_4$ exhibits more positive oxidation potentials than $Tc_2Cl_4(PMe_3)_4$. It might be expected on the basis of electronegativity considerations (Cl being more electron-withdrawing than Br) that $Tc_2Cl_4(PMe_3)_4$ would have a higher oxidation potential than $Tc_2Br_4(PMe_3)_4$. This phenomenon, called the

(42) Hanselman, D.; Smith, T. J. *Polyhedron* **1988**, *7*, 2679–2683.
(43) Brant, P.; Glicksman, H. D.; Salmon, D. J.; Walton, R. A. *Inorg. Chem.* **1978**, *17*, 3203–3206.

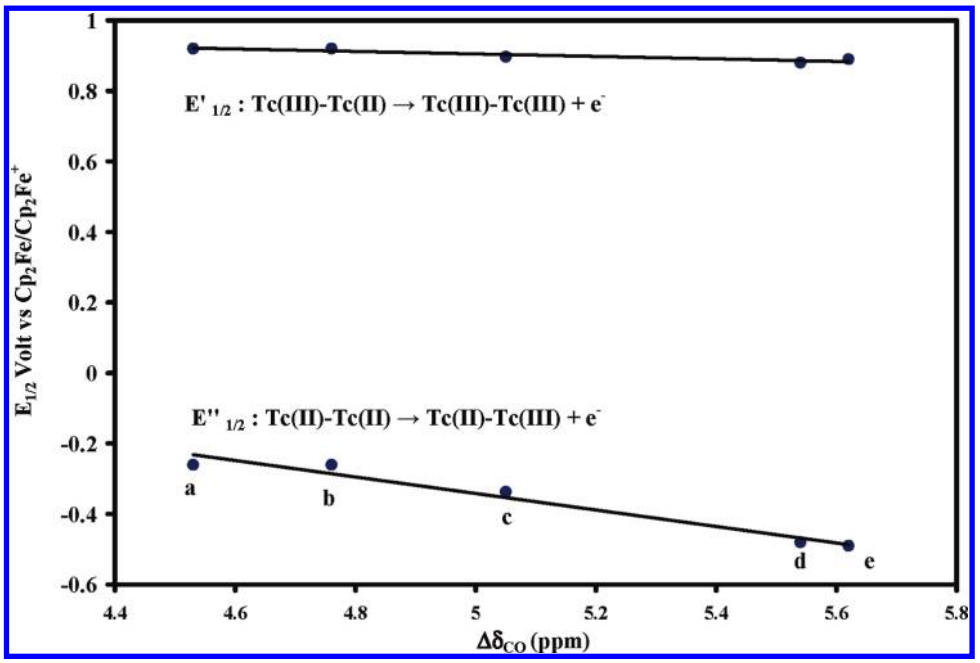

Figure 6. Formal potentials versus $\Delta\delta_{CO}$ (ppm) for the $Tc_2Cl_4(PR_3)_4$ [R_3 = (a) $MePh_2$, (b) Me_2Ph, (c) Me_3, (d) Et_3, (e) n-Pr_3] complexes.

inverse halide order (IHO) effect, has previously been observed for Mo and Re compounds and has been discussed by Gray and co-workers.[45] An explanation for this IHO effect is metal (d) to halide (d) back bonding. Because the metal−metal unit has an electron-rich configuration, the back bonding should increase in the halides series according to I > Br > Cl. It was also proposed for the Re_2(II,II) compounds that the intensity of the IHO effect can be correlated to the degree of metal-to-halide back bonding.[44,45] For the $Tc_2X_4(PMe_3)_4$ (X = Cl, Br), a more significant IHO effect is observed for the oxidation of Tc_2^{4+} than for oxidation of the Tc_2^{5+} unit. The variation of the IHO effect indicates that metal-to-halide back bonding is more important in the Tc_2^{4+} than in the Tc_2^{5+} unit.

The oxidation potentials of $Tc_2X_4(PMe_3)_4$ were also analyzed as a function of energy level of the HOMO, which is the δ^* orbital. Typically, the complex with the lower-lying HOMO is more difficult to oxidize. Our calculations indicate that the HOMO energy levels are stabilized in the order $Tc_2Br_4(PMe_3)_4 > Tc_2Cl_4(PMe_3)_4$, which is consistent with the higher oxidation potential observed for the bromo complex.

The second focus of this study speaks to the influence of phosphines on the redox properties of $Tc_2Cl_4(PR_3)_4$ complexes. Previous studies have shown that $M_2Cl_4(PR_3)_4$ (M = Re, Mo) complexes containing π-acidic phosphines are more difficult to oxidize, and a correlation between oxidation potential and phosphine acidity was established.[42] This phenomenon was explained using metal-to-phosphorus back bonding considerations; i.e., the complexes are more difficult to oxidize as the π-acceptor ability of the PR_3 ligand increases. For technetium, formal potentials of $Tc_2Cl_4(PR_3)_4$ (R_3 = Me_3, Et_3, n-Pr_3, Me_2Ph, $MePh_2$) were plotted as a function of phosphine acidity. Two scales of the π-acidity of phosphines were used, viz., the Tolman[46] and Bodner[47] scales. Analysis of the data using the Bodner scale (Figure 6) indicates that the formal potential associated with the Tc_2^{4+}/Tc_2^{5+} couple increases with phosphine acidity, while little or no effect is observed on the potential associated with the Tc_2^{5+}/Tc_2^{6+} couple. Similar results are obtained using the Tolman criteria (Supporting Information). These results indicate that the phosphine π-acidity is the origin of variation of potentials in the $Tc_2Cl_4(PR_3)_4$ complexes, and this back bonding effect is more important in Tc_2^{4+} than in the Tc_2^{5+} unit.

Using the back bonding considerations previously discussed, we can predict that among the $Tc_2X_4(PR_3)_4$ (X = Cl, Br; R_3 = Me_3, Et_3, n-Pr_3, Bu_3, Me_2Ph, $MePh_2$, Et_2Ph, $EtPh_2$) complexes, $Tc_2Br_4(Me_2Ph)_4$ will be the most difficult to oxidize, while $Tc_2Cl_4(PBu_3)_4$ will be the easiest.

Conclusions

The reactions between $(n\text{-}Bu_4N)_2Tc_2X_8$ (X = Cl, Br) and PMe_3 have been investigated and the triple bonded dinuclear species $Tc_2Cl_4(PMe_3)_4$ and $Tc_2Br_4(PMe_3)_4$ isolated. Along with the Tc(II) dinuclear species, mononuclear Tc(IV) complexes were also detected, which indicated that the mechanism of $Tc_2X_4(PMe_3)_4$ formation involves a disproportionation of the Tc_2^{6+} unit. The structural and spectroscopic properties of the $Tc_2X_4(PMe_3)_4$ complexes have been thoroughly investigated. Both compounds exhibit eclipsed conformations with D_{2d} symmetry, and the metal−metal separations are similar to those found in other $Tc_2Cl_4(PR_3)_4$ complexes, indicating that the change of coordinating phosphine ligand has a minimal effect on the Tc_2^{4+} unit. DFT calculations also demonstrate that the halide ligand has a minimal effect on the bonding in the Tc_2^{4+} unit. The calculated molecular structures of the ground states of $Tc_2Cl_4(PMe_3)_4$ and $Tc_2Br_4(PMe_3)_4$ are in

(44) Brant, P.; Salmon, D. J.; Walton, R. A. *J. Am. Chem. Soc.* **1978**, *100*, 4424–4430.
(45) Zietlow, T. C.; Hopkins, M. D.; Gray, H. B. *J. Am. Chem. Soc.* **1986**, *108*, 8266–8267.
(46) Tolman, C. A. *Chem. Rev.* **1977**, *77*, 313–348.
(47) Bodner, G. M.; May, M. P.; McKinney, L. E. *Inorg. Chem.* **1980**, *19*, 1951–1958.

excellent agreement with the structures determined experimentally. Calculations of effective bond orders for $Tc_2X_8^{2-}$ and $Tc_2X_4(PMe_3)_4$ (X = Cl, Br) indicate a stronger π component in the Tc_2^{4+} core than in the Tc_2^{6+} core. A strengthening of the π bonds leads to a decrease of the metal−metal separation in the Tc_2^{4+} compounds. Electronic spectra of $Tc_2X_4(PMe_3)_4$ exhibit a similar number of low intensity bands that are shifted to lower energy for the Br compound. Assignment of the transitions was performed at both the TDDFT and CASSCF/CASPT2 levels of theory, and the agreement between calculated and experimental values is very good. The redox properties of the dinuclear species were probed by cyclic voltammetry, which shows that both phosphines and halides have an influence on the redox potentials. Analysis of formal potentials indicates that back bonding (metal-to-halide, and metal-to-phosphine) is more important in the electron-rich Tc_2^{4+} unit than in the Tc_2^{5+} unit.

The coordination chemistry of metal−metal bonded Tc complexes is under further development in our laboratories. Current efforts are focused on the synthesis of new quadruply bonded technetium(III) dinuclear species containing tertiary phosphines.

Acknowledgment. The authors thank Mr. Tom O'Dou for outstanding health physics support and Dr. Gordon Jarvinen (Los Alamos) for a generous loan of ammonium pertechnetate. Funding for this research was provided by a subcontract through the U.S. Department of Energy, Office of Science, Office of Basic Energy Sciences, under Contract No. DE-SC0001798, and U.S. Department of Energy, Office of Nuclear Energy, under Contract No. DE-FC07-06ID14781. Use of the Advanced Photon Source at Argonne was supported by the U.S. Department of Energy, Office of Science, Office of Basic Energy Sciences, under Contract No. DE-AC02-06CH11357. Funding for the computation part was provided by the Director, Office of Basic Energy Sciences, U.S. Department of Energy, under Contract No. DE-SC002183.

Supporting Information Available: UV−visible spectra of compounds **1**, **2**, **4**, *trans*-$TcCl_4(PMe_3)_2$, *mer*-$TcCl_3(PMe_3)_3$, *trans*-$[TcCl_2(PMe_3)_4][PF_6]$, *trans*-$TcCl_2(PMe_3)_4$, and $Tc_2Cl_4(PMe_3)_4$. EXAFS spectra of compounds **1** and **4**. Computational details and crystallographic tables, and X-ray crystallographic data in CIF format for $Tc_2Cl_4(PMe_3)_4$. Formal potentials versus ν_{CO} (cm^{-1}) for the $Tc_2Cl_4(PR_3)_4$ complexes. This material is available free of charge via the Internet at http://pubs.acs.org.